RESEARCH ARTICLE
Editor's Choice
ADVANCED MATERIALS
www.advmat.de

Scalable Approach to Molecular Motor-Polymer Conjugates for Light-Driven Artificial Muscles

Xuyang Yao, Jude Ann Vishnu, Claudius Lupfer, Daniel Hoenders, Oliver Skarsetz, Weixiang Chen, Damien Dattler, Alexis Perrot, Wen-zhi Wang, Chuan Gao, Nicolas Giuseppone, Friederike Schmid,* and Andreas Walther**

The integration of molecular machines and motors into materials represents a promising avenue for creating dynamic and functional molecular systems, with potential applications in soft robotics or reconfigurable biomaterials. However, the development of truly scalable and controllable approaches for incorporating molecular motors into polymeric matrices has remained a challenge. Here, it is shown that light-driven molecular motors with sensitive photo-isomerizable double bonds can be converted into initiators for Cu-mediated controlled/living radical polymerization enabling the synthesis of star-shaped motor-polymer conjugates. This approach enables scalability, precise control over the molecular structure, block copolymer structures, and high-end group fidelity. Moreover, it is demonstrated that these materials can be crosslinked to form gels with quasi-ideal network topology, exhibiting light-triggered contraction. The influence of arm length and polymer structure is investigated, and the first molecular dynamics simulation framework to gain deeper insights into the contraction processes is developed. Leveraging this scalable methodology, the creation of bilayer soft robotic devices and cargo-lifting artificial muscles is showcased, highlighting the versatility and potential applications of this advanced polymer chemistry approach. It is anticipated that the integrated experimental and simulation framework will accelerate scalable approaches for active polymer materials based on molecular machines, opening up new horizons in materials science and bioscience.

1. Introduction

Molecular machines are ubiquitous in living nature and can translate their molecular-scale motion into functional macroscale systems using energy to power their operation.[1] The contraction in muscles or the motion of kinesin walkers on microtubules serve as some examples.[2] In the synthetic world, molecular machines can be engineered with great precision to either behave as a molecular switch that cannot accumulate work in reversible operation or as a molecular motor that can accumulate work in continuous, non-reciprocal operation.[3] The light-driven molecular motor based on overcrowded and chiral alkenes as developed by Feringa is the primary contender when thinking about light-powered operation.[4]

One particular challenge toward functional materials is to find pathways that allow to transduce the molecular non-reciprocal motion into macroscopic motion.[3i,5] This has been addressed by the integration of such molecular motors into liquid crystals,[6] into supramolecular

X. Yao, C. Lupfer, D. Hoenders, O. Skarsetz, W. Chen, A. Walther
Life-Like Materials and Systems
Department of Chemistry
University of Mainz
Duesbergweg 10–14, 55128 Mainz, Germany
E-mail: andreas.walther@uni-mainz.de

X. Yao, D. Dattler, A. Perrot, W.-z. Wang, C. Gao, N. Giuseppone
SAMS Research Group
Université de Strasbourg
Institut Charles Sadron – CNRS
23 rue du Loess, BP 84047, 67034 Strasbourg, Cedex 2, France
E-mail: giuseppone@unistra.fr

The ORCID identification number(s) for the author(s) of this article can be found under https://doi.org/10.1002/adma.202403514

DOI: 10.1002/adma.202403514

X. Yao, N. Giuseppone, A. Walther
Freiburg Institute for Advanced Studies
Freiburg, Germany

X. Yao, N. Giuseppone, A. Walther
Strasbourg Institute for Advanced Studies
Strasbourg, France

J. A. Vishnu, F. Schmid
KOMET 1
Institute of Physics
Johannes Gutenberg University of Mainz
D 55099 Mainz, Germany
E-mail: friederike.schmid@uni-mainz.de

N. Giuseppone
Institut Universitaire de France (IUF)
Paris 75005, France

structures,[7] or, as pioneered by parts of us, in chemical organogels and hydrogels.[8] For such gels, it could be shown that crosslinking a tetrafunctional molecular motor with end-functionalized α,ω-telechelic poly(ethylene glycol) (PEG) using alkyne/azide "click" chemistry can lead to light-contractile gels, wherein chains are wound up using the light-driven molecular motors. Engineering of specific photo-modulators has been used to release the strain, and some experimental information has been deduced regarding the influence of chain length, and actuation of gels. However, presently developed crosslinking approaches are prone to network defects, such as loops and dangling chains, and cannot lead to most well-defined quasi-ideal model network topologies that are typically obtained by end-linking star-shaped polymers, for which truly scalable and very facile gelation approaches exist.[9] Network defects such as loops and dangling chains cannot contribute to translating motor rotation into contraction. More importantly, from a fundamental perspective, it would be desirable to have facile control over the polymer type regarding solubility and in particular also chain flexibility to understand whether there are limitations to the operation of such molecular motors when chains become bulky. To this end, the field of molecular machines would greatly benefit from precision macromolecular engineering approaches provided by advanced controlled polymerization techniques.

Here, we address these challenges and introduce the first truly scalable grafting-from polymerization of acrylate-type monomers from a molecular motor core using Cu-mediated reversible deactivation radical polymerization (Cu-RDRP).[10] We demonstrate that these polymerizations can proceed under conditions mild enough to not harm the chemical structure (containing a double bond) of the motor core and that the polymerization is versatile to synthesize different types of polymer chains with different monomer structures and with tunable molecular weight. Additionally, we demonstrate a facile crosslinking approach using the reactive end groups at the terminal monomer units of the star-shaped polymers to crosslink these star polymers into quasi-ideal model networks. Based upon a diversity of samples, we discuss the influence of chain conformational flexibility (different monomers) and chain length on the macroscale contraction kinetics and maximum contraction. Due to the scalable nature of the polymerization and gelation approach, we use these active gels with optimal mechanical performance as artificial muscles and discuss the amount of work performed by such devices. We further develop and use molecular dynamics (MD) simulations of such model networks to shed further light on the experimental results regarding chain length-dependent contraction and the operation of artificial muscles when attaching loads. We believe that this scalable polymerization method toward motor-polymer conjugates with adjustable polymer properties along with reactive end groups opens up opportunities to construct macroscale out-of-equilibrium materials [11] with integrated molecular machines and that it allows to study in great detail the influence of chain architecture on macroscale actuation. Furthermore, our study will inspire the future design of mechanical transmission mechanisms based on highly defined polymer chemistry.

2. Results and Discussion

Our synthetic strategy to prepare well-defined gels with a scalable approach focuses on the grafting-from-polymerization approach from an appropriately functionalized molecular motor core. We opted for Cu-RDRP which allows for the controlled polymerization of a large diversity of vinyl-bond-containing monomers, and which has proven extremely valuable to make well-defined grafting-from processes including star-shaped polymers (**Scheme 1**).[10] To this end, we attached four 2-bromoisobutyrate initiators containing triethylene glycol (TEG) linkers via Cu-mediated click reaction to a tetra-azide functionalized motor core (**Figure 1a**). This motor core is derived from the second generation of Feringa's motors and is able to rotate with high frequencies at room temperature by irradiation at 360 nm (up to the MHz regime in optimized conditions).[8a,12] This synthesis of the resulting 4-armed motor-initiator can be easily scaled up to gram-scale which also guarantees scalable access to the motor-containing star polymers, as well as the following material level study. Below we will show that this method is suitable for different acrylate monomers, but at this point, we first focus on the integrity of the motor core during polymerization conditions.

Since the motor core contains a photo-isomerizable double bond as a rotation center that could potentially react with free radicals, we first investigated the stability of the motor core under conditions similar to a classical radical polymerization by treating a motor-initiator solution (4 μM) with 5 eq AIBN (azobisisobutyronitril) as thermal radical initiator at 70 °C in DMSO. A clear change of the UV–vis spectra occurs in the UV absorption region of the motor, indicating the degradation of the double bond of the motor core when copious amounts of radicals are present (Figure S1a, Supporting Information). This observation prompted us to adopt a specific Cu-RDRP technique [13] that offers very mild conditions with low radical concentrations and operating at 15–20 °C to preserve the structural integrity of the motor-initiator to the best possible extent (Figure 1b, detailed conditions in the Experimental Section). Indeed, compared to the distinct change of the UV–vis spectra of reaction mixtures in classic free radical polymerization conditions (Figure S1a, Supporting Information), in a Cu-RDRP of methyl acrylate (MA) using the motor-initiator (initiator in Figure 1a, conditions discussed below), the UV–vis signal of the motor only shows a minor decrease during the polymerization (Figure 1c). More importantly, the ^{1}H NMR signals surrounding the conjugated bond at the motor core (6.6-8.5 ppm) of a purified motor-polymer conjugate (here a poly(methyl acrylate) (PMA_{50k}); subscript denotes the number average molecular weight, $M_{n,GPC}$, measured by gel permeation chromatography (GPC), see **Table 1**) matches extremely well with those of the non-polymerized motor-initiator (Figure 1d). This confirms the structural integrity of the motor core during the polymerization. To further support this important aspect, we also added a precursor of the motor-initiator ("motor reference", left molecule in Figure 1a) to a Cu-RDRP of methyl acrylate (MA) initiated with the motor initiator and recorded UPLC-MS (Ultraperformance Liquid Chromatography coupled with Mass Spectrometry) to monitor any alterations of the "motor reference" during the polymerization process without actually integrating the

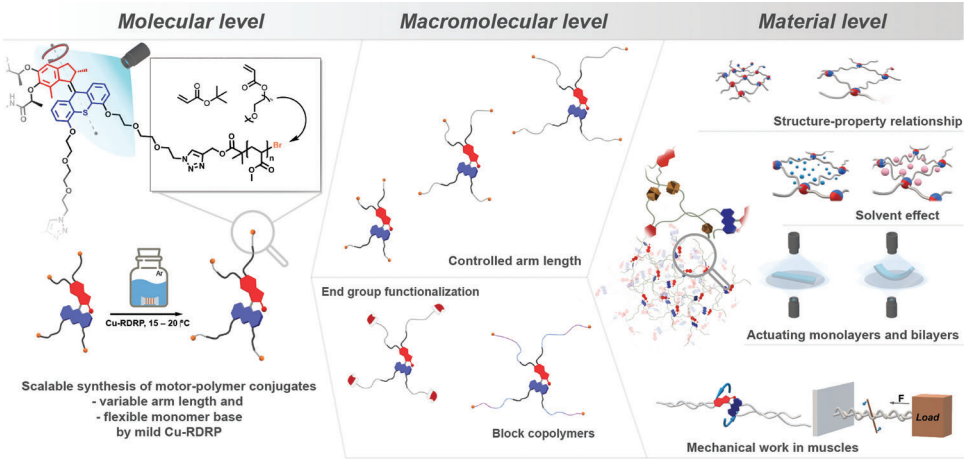

Scheme 1. Overview of the scalable synthesis of motor-polymer conjugates based on the Feringa second generation rotary molecular motor using Cu-RDRP grafting from method. Crosslinking into quasi-ideal networks provides gels to study structure–property relationships and generate light-driven actuators and muscles.

"motor reference" into the polymer chains. The peak corresponding to the "motor reference" of samples taken at different polymerization times could be clearly tracked to remain unaffected on the UPLC chromatograms and its intact mass peak indicates its structural integrity (Figure S1b, Supporting Information). All of these data confirm that the mild Cu-RDRP conditions are not harmful to the double bond of the motor core.

To synthesize a range of different polymers, we developed the Cu-RDRP conditions to suit different vinyl monomers including tert-butyl acrylate (*t*BA), 2-[2-(2-methoxyethoxy)ethoxy]ethyl acrylate (mTEGA), and methyl acrylate (MA). These monomers were selected for showcasing versatility in the polymerization process and for allowing the synthesis of polymers with widely different properties. P*t*BA is a precursor for poly(acrylic acid) – a water-soluble polyelectrolyte with pH-dependent conformation. PmTEGA is a highly soluble polymer that dissolves in many different solvents. PmTEGA has conformationally less flexible chains due to the bulky side groups. PMA is a hydrophobic polymer with a low glass transition temperature (T_g), having the conformationally most flexible chains due to very small side groups. Below we will emphasize on the importance of chain flexibility. Figure 1e–g summarizes the polymerization kinetics obtained for these three monomers at ratios of [monomer]: [motor-initiator] = 1600 (1280 in case of MA) in DMF (for *t*BA and mTEGA) and DMSO (for MA) as solvent and using Me_6-TREN as ligand as well as additional $CuBr_2$ to assist in deactivation of active chains. The first-order kinetic plots show a linear correlation, thus indicating a controlled radical polymerization with constant radical concentration taking place (Figure 1e). Correspondingly, the distribution analysis via GPC shows monomodal peaks that shift to higher molecular weight as the reaction proceeds (blue traces in Figure 1g for PMA). Quantification of the traces shows a linear evolution of molecular weights for all three monomers with narrow dispersities in the range from 1.10 to 1.29 (Figure 1f). The developed strategies allow to synthesize motor-polymer conjugates with precisely controlled molecular weights and in a wide regime of different molecular weights (Figure 1g). The apparent number average molecular weights, $M_{n,GPC}$, determined by GPC can be translated into real arm length by using the calculated $M_{n,calc}$ obtained by relating the conversion during the polymerization following the relationship [monomer]: [initiator] × conversion: 4. Table 1 gives an overview of the maximum arm lengths obtained with these polymerizations and also lists details for the samples used in the following. Overall, the developed strategies allow to synthesize motor-polymer conjugates with precisely controlled molecular weights. Different arm lengths can simply be obtained by sampling from a large reaction mixture or by stopping polymerizations early. Critically, the approach allows highly convenient access to tunable motor-polymer conjugates on a multi-gram scale.

High-end group fidelity regarding the terminal bromine group is an important feature of Cu-RDRP. For our strategy toward the synthesis of gels, high-end group fidelity is important as the gels are formed by arm-to-arm linkages using these end groups. The high end-group fidelity can be directly proven by a chain extension reaction of a motor-PMA_{50k} star polymer with a different monomer, that is, mTEGA, to prepare an amphiphilic PMA_{50k}-*b*-$PmTEGA_{131k}$ block copolymer. Indeed, the GPC traces for the block extension of PMA_{50k} reveal a smooth and consistent shift of the elution peak, confirming that all end groups remain active, even during an intermediate purification step to isolate the motor-PMA_{50k} conjugate prior to the block extension (Figure 1g; orange trace). From a polymer architecture perspective, this also demonstrates an important extension toward more complex amphiphilic structures with a central motor core, for instance, useful to assemble micelles or vesicles in an aqueous solution.[14]

Having confirmed high-end group fidelity, we next turn to the formation of gels. Gel formation was achieved by building on a highly efficient crosslinking reaction between the C-Br end groups at the polymer arms in combination with a dithiol crosslinker (**Figure 2a**).[15] In more detail, the gels were prepared by mixing the motor-polymer conjugates at the corresponding overlap concentration (c*, determined by viscosity measurements, see Figure S2, Supporting Information) with a α,ω-dithiol-functionalized 3,6-dioxa-1,8-octanedithiol

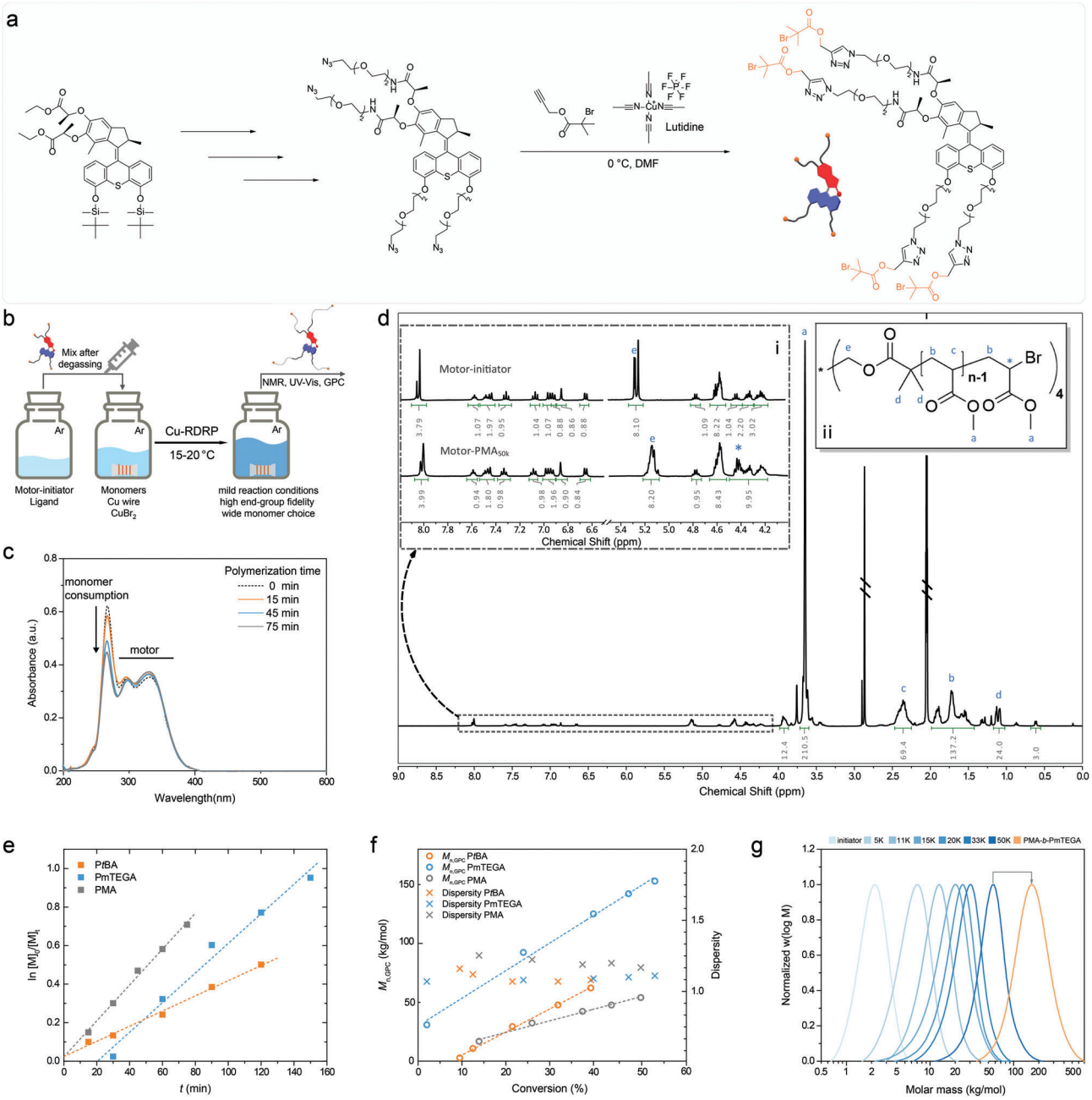

Figure 1. Synthetic strategy toward motor-polymer conjugates via Cu-mediated grafting-from RDRP. a) Synthetic route to 4-arm motor-initiator. b) Illustrative demonstration of Cu-RDRP.c) UV–vis spectra of a reaction mixture during Cu-RDRP of motor-initiator with MA as a monomer. The reaction mixture was diluted to 8.6 μmol L^{-1} in DMSO for the measurement: Conditions: [Monomer]: [motor-initiator] = 1280: 1; 15 °C, DMSO. The decrease of the band located at ≈280 nm arises from the consumption of the monomer during the polymerization. d) ^{1}H NMR of the resultant motor-PMA$_{5k}$-Br ($M_{n,GPC}$ = 5.35 kg mol^{-1}) with magnified details in the aromatic regions surrounding the double bond to confirm the persistence of the chemical structure. e) First-order kinetic plots during a Cu-RDRP of *t*BA, mTEGA, and MA at a ratio of [monomer]: [motor-initiator] = 1600: 1 (*t*BA), 1600: 1 (mTEGA) and 1280: 1 (MA) during polymerization in DMF (for *t*BA and mTEGA) and in DMSO (for MA) at 15 °C. f) Development of apparent $M_{n,GPC}$ and dispersity for the Cu-RDRP in (e). g) Representative GPC elution traces during a Cu-RDRP of MA and during its chain extension with mTEGA.

(DODT) using stochiometric ratios (C-Br/SH) in DMF at room temperature inside of molds, typically generating samples with rectangular dimension ranging from 0.25 × 0.25 cm up to 0.5 × 0.5 cm and with a height of 0.2 to 1 mm (Figure 2b,c). The crosslinking at the overlap concentration minimizes entanglements during crosslinking as well as intra-star crosslinking of two end groups located within one motor-polymer conjugate. This process worked equally well for PmTEGA and PMA motor-polymer conjugates, leading to solid and self-standing gels independent of the molecular weight used.

Table 1. Overview of synthesized motor-polymer conjugates.

Sample code	$M_{n,GPC}$ [kg mol^{-1}] [$Đ$][a)]	$M_{n,calc}$ [kg mol^{-1}][b)]	Arm length[b)]
PMA_{5k}	5.35 (1.19)	4.53	13
PMA_{11k}	10.6 (1.23)	12.2	35
PMA_{15k}	15.1 (1.29)	14.3	41
PMA_{20k}	19.8 (1.20)	18.4	52
PMA_{33k}	32.5 (1.19)	29.6	84
PMA_{50k}	49.6 (1.18)	50.1	144
$PtBA_{62K}$[c)]	62.1 (1.08)	79.9	156
$PmTEGA_{153k}$[c)]	153 (1.11)	185.1	212
PMA_{50k}-*b*-$PmTEGA_{131k}$	148 (1.24)	181.2	144 MA + 150 m(TEGA)

[a)] Obtained by GPC in DMAc using PMMA standards for calibration; [b)] Calculated by the degree of conversion obtained from ^{1}H-NMR tracking the monomer consumption (MW of the motor core is not included); [c)] Only the sample with the largest molecular weight is provided; shorter ones can be isolated by sampling.

Afterward, these gels were typically allowed to swell to the equilibrium degree of swelling before further characterization of their contractability.

Using these gels, we investigated the material level behavior regarding macroscopic contraction under UV irradiation at 365 nm. To our great surprise, organogels composed of motor-PmTEGA did not show any obvious light-induced contraction, independent of the molecular weight (≈30, 90, 120, and 153 kg mol^{-1}), solvent (H_2O, DMF) or irradiation power used (≈1, ≈6, and ≈30 mW cm^{-2}). In contrast, motor-PMA systems showed consistent contraction under UV irradiation (e.g., in acetone, THF, or toluene; (Figure 2c)). This is a noteworthy result, because it demonstrates for the first time the importance of chain flexibility (e.g., expressed for instance via the persistence length, $L_{p,\,PEG}$ = 0.38 nm,[16] $L_{p,\,PMA}$ = 1.05 nm, for comparison $L_{p,\,polydecylacrylate}$ = 2.60 nm [17]), and side-chain volume: PmTEGA ≫ PMA) on the appearance of a molecular motor-induced contraction process. Previous systems had only considered ultra-flexible polyethylene glycol (PEG).[8b–d] We hypothesize that the mTEGA side chains act as geometric and energetic obstacles to the winding up process of the polymer chains responsbile for gel contraction. PMA chains contain the smallest possible side groups of all acrylate monomers with organo-solubility.

Since the Cu-RDRP allows for a simple tuning of the degree of polymerization of the motor-PMA star polymers, we systematically studied the influence of the arm length on the gel properties and their contraction for samples bridging from PMA_{11k} to PMA_{50k}, hence equaling a degree of polymerization of 35 to 144 units in each arm (Table 1). To gain further insights into the gel structure, we performed compression mechanical analysis after allowing the gels to swell to an equilibrium degree of swelling. Figure 2d shows that the compressive moduli (E) of the swollen gels scale in a power law relationship of $E \approx M_n^{-1.1}$, indicative of a defined network. In addition, the uniform crosslinking of the network is also evidenced by the measurement of swelling ratio (Q), where $Q = 1/\nu_2$ with ν_2 representing the volume fraction of polymer in the swollen gel. Q of gels with varied arm lengths exhibit a power law correlation of $Q \approx M_n^{0.7}$, again confirming a quasi-ideal network topology.[18] The confirmation of the presence of a quasi-ideal model network topology is important because it allows to study the influence of the motor on the contractibility of the overall gels without excessive sample-dependent network defects.[8c]

We performed quantitative studies on the time-dependent contraction of gels containing motor-PMA for samples prepared at 0.25 × 0.25 cm with a thickness of ≈200 µm and after reaching their equilibrium degree of swelling in acetone during two-sided UV irradiation with a total intensity of 1.4 mW cm^{-2} (Figure 2b,e). Interestingly, we find that the gels show a non-linear dependence of the initial rate of contraction, with gels based on an intermediate molecular weight showing the fastest initial contraction. In contrast, all gels contract to a similar contraction value of ≈20% decrease in area. The latter result clearly shows that the total contraction is independent of the network junction length/arm length, indicating that the total contraction ratio is rather a total function of the supercoiled structure of the arms with similar topological limitations with limited impact of the presence of the motor core. The difference in early contraction relates most likely to the balance between the optical density of the films, and the amount of motors that lead to different kinetics of contraction. In theory, more motors should lead to a faster contraction, but on the other hand, more motors also imply a higher optical density and a higher degree of crosslinking that might both be adversarial to fast contraction.

In order to obtain a clearer understanding of the process of gel contraction induced by the rotation of the motors, we implemented an MD simulation [19] framework for coarse-grained polymer networks with motor-like crosslinkers (details of the simulation routine can be found in Figure S3, Supporting Information). In analogy to the experimental systems, we considered tetra-functional crosslinking units as motors (red beads) embedded in the topology of a diamond lattice (Figure 2f). They are connected via linear spring-bead chains [20] with varying lengths (green, N_s = 21, 40, 62, 84). We employed a six-bead representation for the motors, where two rigid rod-like subunits [21] comprising three beads each can be driven to rotate with respect to each other (see Figure 2h, inset). Since the experimental time scales of contraction are in the range of minutes (Figure 2e) and thus much longer than typical polymer relaxation times, we conducted the simulations such that the gel was allowed to relax to equilibrium between motor rotations. The simulation thus consisted of a sequence of rotation and relaxation steps: In each rotation step (rotation half-cycle), a torsional force (using an

asymmetric dihedral potential, see Supporting Information for details) was applied to the motors such that they could rotate by 180° unless the restoring tension forces from the attached polymer strands were too high. In the relaxation step, the motor structure was fixed and the gel relaxed to a new equilibrium state. These simulations capture the macroscopic contraction of the gel and also the mesoscale winding up of individual chains as can be seen in Videos S1, S2 (Supporting Information) and Figure 2g.

Initially, during the first rotation cycles, practically all motors undergo rotation during rotation steps. With time, as the strands wind up, more and more motors stall. This is demonstrated in Figure 2h which shows the fraction of motors that undergo a 180° rotation during a rotation half-cycle as a function of time (lower axis) or number of rotation cycles (upper axis). This fraction is initially close to one, but then decays rapidly and approaches zero at late times. More and more motors stall, because the applied torque is not sufficient to overcome the strong opposing internal torque generated by the twisted chain pairs that are attached to the motor. In systems with shorter arms and thus a higher density of motors (e.g., $N_s = 21$) the motors stall earlier, whereas the stalling occurs later in systems with longer arms and lower density of motors. Even though the curves look similar in their decay profile, they cannot be collapsed onto one master curve upon rescaling and shifting. This reflects the topological constraints imposed by the motor crosslinks in relation to the length of the polymer chains that can be wound up.

To quantify the total contraction of the gels, we calculate the squared gyration radius of the gel, defined as $\langle R_g^2 \rangle = \frac{1}{N}\langle \sum_{i=1}^{N} |r_i - r_{cm}|^2 \rangle$, as a function of time. Here, r_i is the position of the i^{th} monomer, r_{cm} the position of the center of mass of the gel and the average $\langle ... \rangle$ runs over 4 independent simulation runs. Figure 2i shows the ratio of $\langle R_g^2 \rangle$ at time t and at time $t_0 = 0$, termed "size ratio", as a function of time. Clearly, the contraction speed depends on the number density of molecular motors in the sample and is the fastest for the sample with the shortest strand length ($N_s = 21$). In the experiments (Figure 2e), the initial speed of contraction depends on the average strand length in a non-monotonic manner: It first increases and then decreases again. The simulations do not show such a non-monotonic behavior, the contraction speed consistently increases with decreasing strand length (Figure 2i). This discrepancy can be understood from the fact that the simulations do not account for the effects of increased optical density at high motor concentration, limiting penetration of the light into the material. At late times, the total relative contraction is similar in all samples. This is in qualitative agreement with Figure 2c, however, the actual values of the total contraction differ – the final contraction level is much higher in the simulations than in the experiments. We will discuss this further at the end of this section.

Given the scalability of the overall approach, interesting questions can be asked for establishing macroscopic behavior, in particular regarding the construction of light-driven muscles useful in soft robotics. The above data brings about the intriguing conclusion that gels with higher crosslinking density would be better candidates for macroscopic mechanical performance because higher crosslinking density leads to higher mechanical stiffness (e.g., elastic modulus) while similar relative contraction ratios can be achieved rather independently of the concentration of the molecular motor. Critically, just increasing the concentrations of the components above c* is not appropriate to increase mechanical properties as physical entanglements hinder contraction,[8c] whereas the strength of our approach is to increase the polymer concentration using simply motor-star-PMA with lower arm length while maintaining c*. These considerations are for instance important when aiming for lifting cargo, which we will demonstrate below. Some first interesting behaviors regarding actuation can be observed from the PMA_{11k} motor-gel under UV irradiation. Different from motor-gels composed of higher molecular weight polymers, the PMA_{11k} motor-gel shows a flapping motion under single-sided UV irradiation (**Figure 3a**, gels prepared at 0.5 × 0.5 cm and 200 µm thickness, acetone, 365 nm, 0.7 mW cm^{-2}, Video S3, Supporting Information), rather than a simple 2D contraction observed for motor-gels with lower crosslinking density. This behavior can be explained by the fact that the UV irradiation intensity decreases according to the Lambert Beers Law in the gel film (Figure S4, Supporting Information). It is the macroscopic manifestation of the reasons for the non-linear dependence of the contraction rate as discussed for Figure 2e, where we however used two-sided illumination to minimize as best as possible the build-up of optical gradients. Here during one-sided illumination, the gel parts located on the side of the light source undergo contraction first before they reach their topological limitations, whereafter the more slowly contracting part at the other side of the gel catches up. It shows that the kinetics of contraction can be influenced by material-embedded "shading" or attenuation effects. This is most evident for motor gels with high crosslinking density, hence high density of absorptive motor units, whereas gels containing higher arm length do not show this behavior at similar light intensity and material thickness.

Constant bending, without subsequent flattening, can be achieved by designing double-layer gels. These were obtained by first crosslinking an active gel of a motor-PMA_{11k} star polymer in a rectangular mold (1.0 × 0.2 cm with 0.2 mm thickness), followed by transferring the crosslinked gel into a second rectangular mold (1.0 × 0.2 cm with 0.4 mm thickness) and filling up the rest of the mold with non-motor PMA_{11k} star polymer, based on a conventional 4-arm initiator without motor, and crosslinking it with the difunctional thiol (Figure 3b). After transfer to an acetone bath, some initial selective swelling of the non-motor layer occurs, leading to some pre-bending. Upon light irradiation, substantially more directional bending occurs, and the bending persists over time due to the mechanically durable interface and the inactive nature of the passive layer. The opening angle from the center of the body to the two "arms" changes from ≈98° to ≈57° during the contraction. Video S4 (Supporting Information) shows an inverted design where the "arms" contract with frictional sliding over a surface. A related device (2.0 × 0.2 × 0.15 cm) with 67% active layer and 33% passive layer (in regards to the thickness) is easily able to lift an object with a weight of ≈78 mg under UV irradiation, hence corresponding to ≈100 times the dry mass of the motor active/non-motor inactive bilayer gel (Figure 3c, Video S5, Supporting Information). The bending is less pronounced because of the weight, and the different thickness dimensions. Below we discuss the maximum load that can be lifted in a 1D muscle configuration.

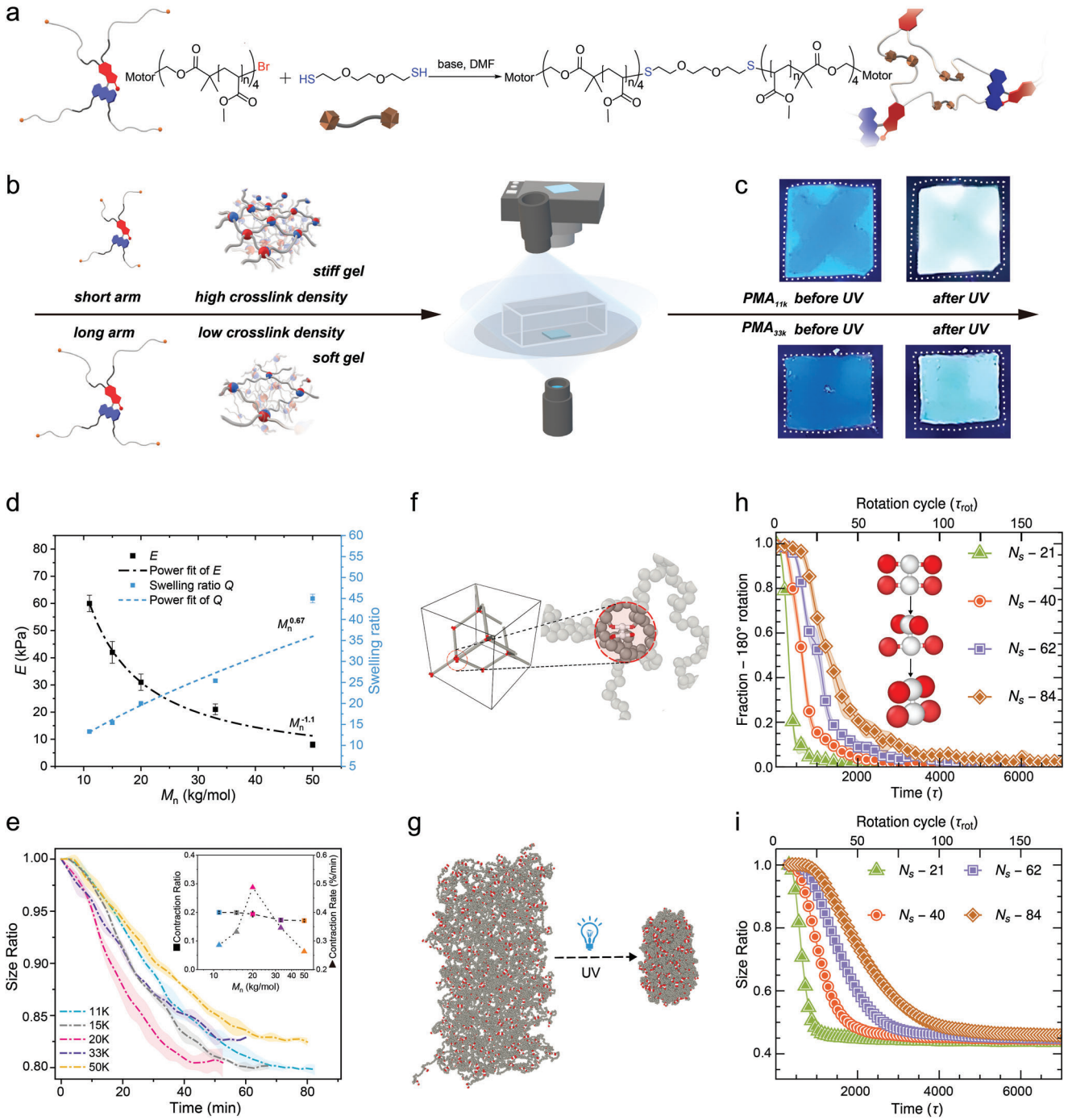

Figure 2. Light-driven contractability of molecular-motor gels with different arm lengths. a) Illustration of the crosslinking process by nucleophilic substitution reaction between C-Br and an α,ω-containing dithiol. b) Illustration of the influence of the arm length of motor-polymer conjugates on hydrogel structure with different crosslinking densities. c) Organogels of PMA_{11k} and PMA_{33k} in acetone at equilibrium swelling show similar contraction after exposure to UV. Gel dimensions 25 mm × 25 mm × ≈200 µm. Two-sided irradiation with 1.4 mW cm^{-2}. The faint cross in the background is a marking in the petridish for observation. d) Correlation between elastic compression moduli (E) of equilibrium swollen gels in acetone, and of the swelling ratio (Q) after gel formation in DMF at the individual overlap concentration and subsequent transfer to acetone. e) Time-dependent contraction expressed as 2D size ratio during UV irradiation experiments of equilibrium swollen, crosslinked gels with varied molecular weights of motor-PMA in acetone. The curve represents an average of 3 independent samples with the shaded area being the standard deviation. The inset shows the contraction rate at early linear stages, as well as the total contraction ratio in percent of the area lost. f,g) Schematic illustration for the initialization of the gel for simulations using a regular diamond network model: motors in red, polymer chains in green. Real simulation snapshot during an exemplary contraction simulation when rotating the motors in the polymer network. h) Plot showing the fraction of molecules that can rotate by 180° as a function of time in simulation units τ (inset shows process of motor rotation). N_s = strand length. i) Time-dependent contraction expressed in terms of the size ratio, which is defined as the ratio of radii of gyration $\langle R_g^2(t)\rangle^{\frac{1}{2}} / \langle R_g^2(0)\rangle^{\frac{1}{2}}$.

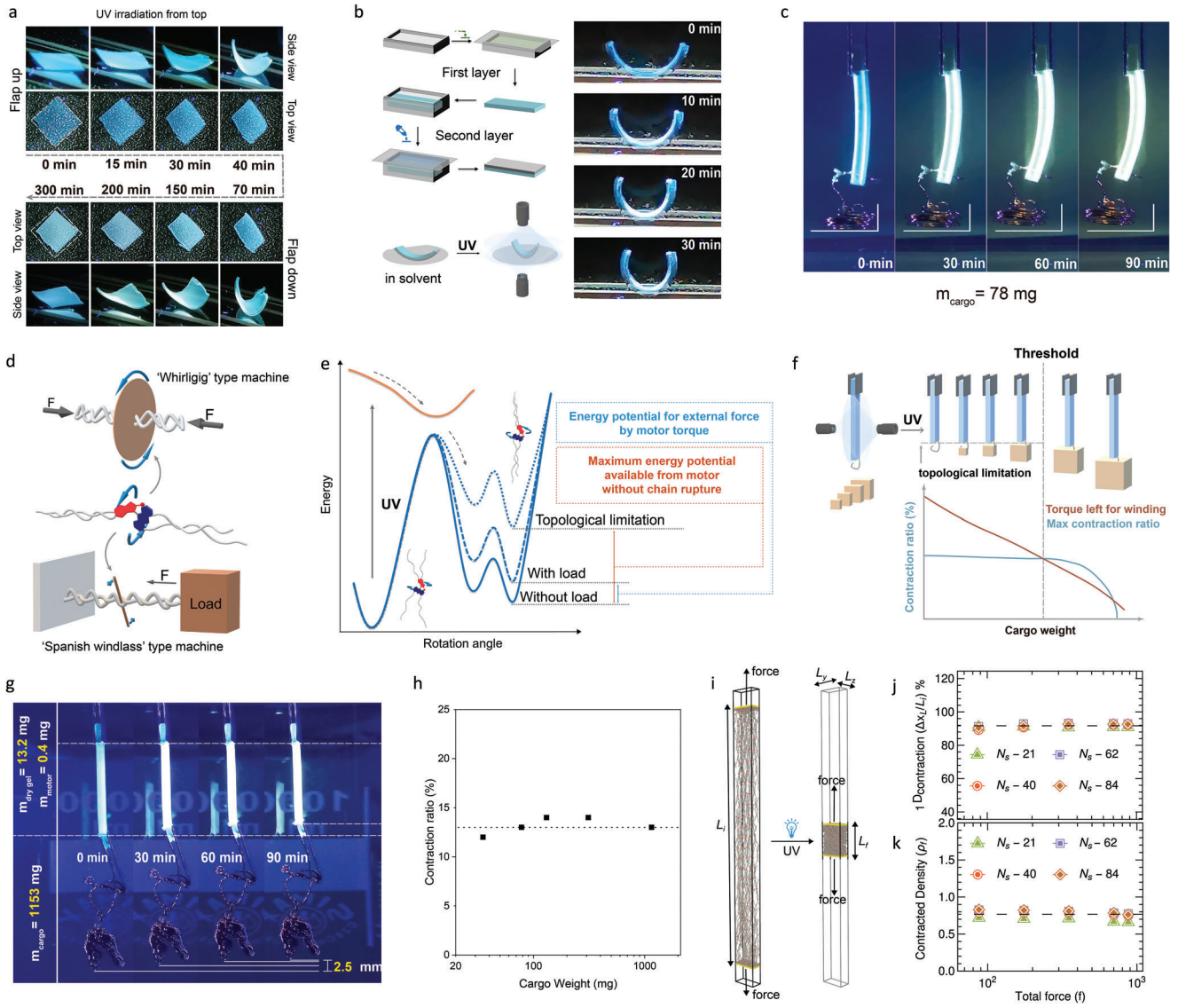

Figure 3. Motor-polymer-based gels as artificial muscles. a) Transient bending motion of motor-PMA$_{11k}$-gel under UV irradiation from top (0.5 × 0.5 cm and 200 µm thickness, acetone, 365 nm, 0.7 mW cm^{-2}, Video S3, Supporting Information). b) Persistent bending behavior of a bilayer soft robotic device with designed active (motor-PMA$_{11k}$-gel, top layer) and inactive layers (non-motor-PMA$_{11k}$-gel) under UV irradiation (365 nm, 0.7 mW cm^{-2}). Total dimensions are 1.0 × 0.2 cm with 0.2 mm thickness for active and 0.2 mm thickness for inactive layer (acetone). Video S4 (Supporting Information) shows an inverted design where the "arms" touch the surface. c) Moving a cargo with a weight of ≈78 mg by UV-powered bending of the bilayer motor gel. Total dimensions are 2.0 × 0.2 cm with 1.0 mm thickness for the active layer (PMA$_{20k}$-gel) and with 0.5 mm for the inactive layer (non-motor PMA$_{20k}$-gel). The load is attached by poking a wire through the gel (Video S5, Supporting Information). d) Cartoon illustration of the "Whirligig"-type and "Spanish Windlass"-type machines fabricated based on a molecular motor with unidirectional working mode. e) Illustration of energy landscapes showing the different working cases of the "Spanish Windlass" type machine, including with/without load and considering the existence of topological limitations at highly wound-up chains. More details on the ratchet mechanism can be found in ref. [3c] f) Cartoon illustration of the topological limitation of the "Spanish Windlass" type machine in cargo lifting experiments. g) Experimental demonstration of the "Spanish Windlass" type machine in cargo lifting experiments for motor-PMA$_{11k}$-gel. Dimensions are 2.0 × 0.5 cm with 1.5 mm thickness (THF, Video S6, Supporting Information). h) Experimental results indicating the existence of topological limitation when cargo weights are below the critical value in cargo lifting experiments. i) Simulation snapshots for a 1D contraction under applied load. j,k) Plots of 1D contraction in percent and of the density in the contracted state as a function of applied loads. Simulation data are given in simulation units of k_BT and bead size (Video S7, Supporting Information).

An intriguing question then arises for whether it is possible to evaluate how much torque the motors could generate and transmit into macroscopic force for performing work. In one of the recent works,[24] motor-embedded polymer networks were designed to work as nanomachines similarly like a "Whirligig" handcraft toy, in which the energy could be stored and afterward released when the torque applied on the wheel was removed (Figure 3d–f). In analogies of our real life, one could find similar structures in a traditional hand-built tool, a "Spanish Windlass", in which the torque applied from the stick for twisting the

ropes will sustain until the ropes reach a topological limitation. In this process, the machine will generate a force pulling the cargo attached at the active end of the ropes. Once the ropes are too tightly wound, the external torque no longer suffices for further contractions. This operational principle resembles the scenario in our motor-gel. Specifically, when one end of a gel strip is fixed by clamps and the other end is loaded with cargo (copper wire with a certain weight in our experiments), every motor in the gel works similarly like in a "Spanish Windlass" in a joint manner. As discussed above, because of the topological limitation, the gel can only contract to a certain ratio (≈20%) (Figure 3f). This suggests that, by increasing the cargo weight, it is possible to determine the critical weight above which the motors could no longer provide extra torque to twist the polymer chains to reach the topological limitation. Experimentally, we increased the cargo weight and measured the contraction (Figure 3g,h, Video S6, Supporting Information). We found that a motor gel containing ≈13 mg motor-PMA_{11k} – and thus ≈0.4 mg motor core – can lift a buoyancy-corrected cargo weight of up to 1.15 g to the same constant contraction value as for lower weights. This is already an impressive lifting of ≈2800 times of the mass of all motors, or ≈100 times the dry mass of the artificial muscles. Unfortunately, it is not possible to determine the critical point of cargo weight, because heavier cargos cause fracture of the motor-gel after a certain time of contraction. Based upon the load of 1.15 g, we can calculate a total force of 1.13×10^{-2} N, which corresponds to 1.59×10^{-11} nN per motor acting truly on lifting the mass. Interestingly, this maximum force per motor correlates to scaling considerations of molecular motors.[22] Hence, it is rather the proneness to material fracture rather than the maximum force of the motor that limits the actuation as an artificial muscle at this point.

We also complement these experiments with further simulations by examining the contraction of the gels under different loads. The corresponding setup is shown in Figure 3I (Video S7, Supporting Information). The gel is attached to plates (yellow) at two sides, which are pulled apart by a constant force, mimicking the effect of the load force.[23] Periodic boundary conditions are applied in the two directions perpendicular to the plates. Initially, we apply this pulling force to the gel without allowing the motors to rotate. The length of the gel slab expands from the initial (force-free) value L_0 to a total length $L_i = L_0 + \Delta L$. The relative extension $\Delta L/L_0$ is proportional to the applied force for small forces, and then saturates (see Supporting Information, Figure S5a, Supporting Information). We restrict the range of forces to the initial linear, Hookean regime. Then we apply cycles of motor rotation and relaxation steps as described above. As a result, the gel contracts to a final length L_f. From the displacement of the plates, we can calculate the 1D contraction ratio, $\Delta x_L = 1 - \frac{L_f}{L_i}$ as a function of applied load (total force) for gels with different N_s. Figure 3j shows that the contraction ratio is largely independent of both N_s and the total force, in agreement with the experimental results of Figure 3g. However, the absolute value of this limiting relative contraction is again much larger in the simulations than in the experiments, like for free gels (Figure 2i).

The question arises which physical effect limits the relative contraction. One might hypothesize that the limiting factor is excluded volume, that is, the gel cannot contract beyond a certain critical density. To test this hypothesis, we plot the monomer number density, ρ_f, of the gel in the contracted state (Figure 3k). It is similar for different strand lengths and forces, but the spread is higher, particularly for small strand lengths. To assess the limiting density set by volume constraint, we determined the density as a function of compression in a gel with non-rotating crosslinking molecules (Figure S5b, Supporting Information). The results reveal that the limiting density values in the contracted gels are by no means special, they are in fact much lower than the maximum density at high compression. Therefore, we conclude that excluded volume is not the factor that limits gel contraction. It is in fact limited by topological restrictions, as suggested by chemical intuition earlier.[8d] Our simulations however set this now on a solid computational basis. A second question is why the contraction ratios achieved in the simulations are so much higher than in the experiments. In the simulations, we consider an idealized situation where motors are not allowed to unwind back once they have rotated. In reality, unwinding is possible and can be observed, and the ground state activation barrier of E/Z isomerization for unwinding has been estimated to be 46 k_BT.[24] We have estimated the distribution of torques at the end of the final relaxation step, which are transmitted to the motors by the attached entangled and twisted chains, and are counterbalanced by the strong dihedral potential. They can reach values of up to 120 k_BT, even though the average torque value per motor is much smaller (of order 20 k_BT). In a more realistic model, a significant fraction of motors would unwind, which will presumably greatly reduce the maximum contraction. The influence of a finite activation barrier for unwinding on the limiting contraction rate will be studied in future work.

3. Conclusion

In this study, we have introduced a versatile and scalable approach for integrating light-driven molecular motors into polymeric materials, leveraging advanced polymer chemistry techniques based on controlled/living radical polymerization. A key aspect of our methodology involves Cu-mediated RDRP, which ensures low radical concentrations, preventing unwanted side reactions, especially with the photo-isomerizable double bond of the molecular motor. Through this technique, we have demonstrated precise control over the growth of polymer arms from the molecular motor, including control over arm length and the chemical nature of these arms, and including block copolymers. This breakthrough significantly expands the range of materials available for incorporating molecular machines into polymeric matrices.

The high-end group fidelity of our polymerization method has enabled subsequent crosslinking into gels using straightforward crosslinking reactions. This process yields quasi-ideal network topologies, facilitating a fundamental understanding of light-induced contraction mechanisms driven by the winding of molecular motor chains. Our experiments revealed that while similar total contraction ratios were achieved, the contraction speed exhibited non-linearity dependent on motor density due to the compromise between optical density, light attenuation, and motor density. To gain deeper insights, we developed an MD simulation framework that accurately captured the essence of

light-induced contraction. Our simulations clarified that the experimentally observed non-linearity in contraction speed arises from sample thickness effects, whereas the computer simulations show that a higher density of molecular motors indeed leads to continuously faster contraction kinetics. The total contraction ratio remained constant in both experimental and simulation data for different arm lengths, confirming that the motor concentration only has a limited impact. Simulations clearly show that the total contraction is indeed limited by topological limitations and not excluded volume effects as substantial amounts of solvent remain in the final contraction state.

Leveraging the scalability of our motor-polymer conjugate synthesis and gelation methods, we demonstrated the potential of these materials as artificial muscles capable of cargo lifting, bending, and actuation. These load-lifting artificial muscles exhibited impressive performance, lifting up ≈100 times of their solid body weight. They do not yet reach a load-limiting scenario where the torque of the motor is insufficient to lift attached materials, because fracture of the material at the load attachment site occurs. This may in the future however be addressable using other polymer gel network concepts, such as double network hydrogels.

Looking ahead, our advanced polymer chemistry approach for integrating light-driven molecular motors presents exciting prospects for accelerating the development of large-scale active polymer materials. The synergy between experimental and simulation efforts offers a comprehensive understanding of these systems. Yet, several open questions persist, such as exploring simulations at lower torque and considering polymer chains with more chemical details influencing steric crowding and persistence length. Furthermore, future investigations could focus on polyacrylic acid, where simple pH and salinity adjustments profoundly impact chain conformation. Our initial synthetic exploration of amphiphilic block copolymers holds promise for designing solution-based structures like polymersomes, with tunable bilayer membrane permeability dependent on arm length and light exposure. Additionally, the synthesis and gelation concepts developed here may find application in other molecular machine systems with sensitive components.

4. Experimental Section

Materials, selected methods, and the synthesis of the motor component are documented in the Supporting Information.

Cu-Mediated Polymerization: A typical polymerization works as follows: copper wire (20.0 cm) was wrapped around a cross magnetic stirring bar and activated by stirring in concentrated hydrochloric acid solution for 30 min. The copper wire was rinsed with acetone, dried in an N_2 flow, and directly added to a Schlenk flask A containing 239.0 mg methyl acrylate (MA), 0.097 mg $CuBr_2$ and 2730 µL DMSO. DMF (20 µL) was added as an internal reference for NMR. Moto-initiator (4.33 mg) and 0.360 mg Me_6-TREN was added in 2000 µL DMSO in Schlenk flask B. Each solution in Schlenk flask A and B was degassed with N_2 for 20 min to remove dissolved oxygen. After degassing, the solution in Schlenk bottle A was transferred into Schlenk bottle B using an N_2-inerted syringe. The reaction temperature was maintained at 15 °C and the magnetic stirring was kept at 500 rpm. Aliquots of the reaction mixture were taken out during the polymerization by N_2-inerted syringe and analyzed by NMR to calculate the monomer conversion. The polymerization was quenched by adding deionized water into the reaction mixture. The motor-PMA was extracted by DCM and washed 3 times by deionized water. The residual methyl acrylate was removed by rotary evaporation. The final motor-PMA product was free-dried overnight to remove residual solvents including DMSO.

Preparation of Motor-Gel Samples: The motor-polymer conjugate of choice, 3,6-dioxa-1,8-octanedithiol (DODT), and the *N*-Methyl-1,3-diaminopropane were separately dissolved in DMF in desired concentrations before mixing to guarantee the stochiometric ratios of C-Br/SH and the motor-polymer conjugated at corresponding overlap concentration (determined by viscosity measurements, see Figure S2, Supporting Information). Specifically, for motor-polymer motor-PMA_{11k}, 30 mg motor-PMA_{11k} was dissolved in 150 µL DMF in a 2.5 mL plastic centrifuge vial. DODT was prepared as a stock solution in DMF at the concentration of 2.0×10^{-4} mol L^{-1}. The *N*-Methyl-1,3-diaminopropane was prepared in DMF at the concentration of 4.0×10^{-2} mol L^{-1} as stock solution. Afterward, 22.5 µL of DODT stock solution and 24.2 µL of *N*-Methyl-1,3-diaminopropane stock solution were added into the vial containing motor-PMA_{10k} DMF solution. The solution was vortexed followed by centrifugation to remove any bubbles. The solution was then transferred into the mold made by CNC milling with the desired size, sealed by a coverslip, and left at room temperature overnight for complete crosslinking. The crosslinked motor-gel was carefully peeled off from the mold using a spatula and transferred into a solvent reservoir for solvent exchange (e.g., acetone, THF) and to remove any excess *N*-Methyl-1,3-diaminopropane.

Determination of Compressive Moduli (E) and Swelling Ratio (Q): The compressive moduli (E) of the gels were measured by an Anton Paar 702e Dynamic Mechanical Analysis (DMA) in compression mode using a plate-plate (PP50) measuring system. The motor-gel was prepared within a mold (0.5 cm × 0.5 cm with 1 mm thickness) followed by swelling in DMF to an equilibrium state. The size of the gel was measured by a brightfield microscope. Compressive moduli (E) were obtained through compression mode with frequency sweeps from 0.1–10.0 Hz with 1.0% strain.

Swelling ratio (Q), $Q = 1/\nu_2$ with ν_2 representing the volume fraction of polymer in the swollen gel, was calculated by converting $Q = 1/\nu_2$ into $Q = \frac{(m_{swollen\ gel} - m_{dry\ gel})/\rho_{DMF}}{m_{dry\ gel}/\rho_{polymer}}$ in which the $\rho_{polymer}$ was determined as ≈1.1 g cm^{-3} for motor-PMA samples by weighing the weight displacement of water after submerging polymer samples hanging by a thread based on the Archimedes Principle.[25]

UV Irradiation Experiments on Motor-Gel Samples for 2D Contraction Measurement: The swollen motor-gel was transferred into a quartz cuvette which was then sealed with a rubber stopper and filled with acetone. The cuvette was placed flat on a PS plastic petri dish with one 365 nm UV lamp on top and the other one underneath the petri dish. Each UV lamp was set to provide 0.7 mW cm^{-2} irradiation power on the spot where the cuvette was placed. Note that the UV lamp on top was tilted with a small angle so as not to block the camera to record the video during motor-gel contraction under irradiation. Image frames in the video corresponding to a certain irradiation time were extracted and the gel sizes were measured by ImageJ. 2D contraction ratios were calculated using the area of the gel at the corresponding frame divided by the initial value.

UV Irradiation Experiments on Motor-Gel Samples for Double-Layers Gel Bending: The swollen double-layer motor-gel was transferred into a quartz cuvette which was then sealed with a rubber stopper and filled with acetone. The cuvette was placed flat on a PS plastic petri dish with one 365 nm UV lamp on top and the other one underneath the petri dish. Each UV lamp was set to provide 0.7 mW cm^{-2} irradiation power on the spot where the cuvette was placed. The camera was set up on one side for video recording with a side view.

UV Irradiation Experiments on Motor-Gel Samples for Cargo Lifting: The double-layer motor-gel was first swollen in DMF to avoid solvent evaporation during manipulating and fixed with one end by a metal clamp. One bunch of copper wires with a certain weight as a cargo load was attached by poking one end of the wire through the gel. This assembly was then transferred into a 1000 mL beaker filled with THF for solvent exchange. Two UV lamps were set on the left and right sides of the beaker, each providing 5 mW cm^{-2} irradiation power on the beaker wall. The camera was set up on one side of the experimental setup for video recording with a vertical side view. Image frames in the video were extracted and the displacement of the cargo was measured.

Supporting Information

Supporting Information is available from the Wiley Online Library or from the author.

Acknowledgements

X.Y. and J.A.V. contributed equally to this work. Funding from the German Science Foundation is acknowledged: A.W. and F.S. are members of the RTG 2516 (Grant No. 405552659) and J.A.V. is the recipient of a doctoral position within the RTG 2516 program. A.W. and N.S. acknowledge the support of USIAS and FRIAS Institutes for Advanced Studies in Strasbourg (France) and Freiburg (Germany). A.W. acknowledges funding from the European Research Council via a Consolidator Grant (101001638) and from Gutenberg Research Professorship underpinning his "Life-Like Materials Program". Parts of this research were conducted using the supercomputer MOGON 2, which is a member of the AHRP (Alliance for High Performance Computing in Rhineland Palatinate, www.ahrp.info) and the Gauss Alliance e.V. The authors gratefully acknowledge the computing time granted on the supercomputer MOGON 2 at Johannes Gutenberg University Mainz (hpc.uni-mainz.de).

Open access funding enabled and organized by Projekt DEAL.

Conflict of Interest

The authors declare no conflict of interest.

Data Availability Statement

The data that support the findings of this study are available from the corresponding author upon reasonable request.

Keywords

controlled radical polymerization, gels, life-like materials, molecular machines, molecular motors, photochemistry, soft robotics

Received: March 8, 2024
Revised: April 9, 2024
Published online: April 21, 2024

[1] M. Schliwa, G. Woehlke, *Nature.* **2003**, *422*, 759.
[2] a) I. Rayment, H. M. Holden, M. Whittaker, C. B. Yohn, M. Lorenz, K. C. Holmes, R. A. Milligan, *Science.* **1993**, *261*, 58; b) R. D. Vale, R. A. Milligan, *Science.* **2000**, *288*, 88.
[3] a) S. Erbas-Cakmak, D. A. Leigh, C. T. McTernan, A. L. Nussbaumer, *Chem. Rev.* **2015**, *115*, 10081; b) B. L. Feringa, *Angew. Chem., Int. Ed.* **2017**, *56*, 11060; c) S. Kassem, T. van Leeuwen, A. S. Lubbe, M. R. Wilson, B. L. Feringa, D. A. Leigh, *Chem. Soc. Rev.* **2017**, *46*, 2592; d) D. Roke, S. J. Wezenberg, B. L. Feringa, *Proc. Natl. Acad. Sci. U. S. A.* **2018**, *115*, 9423; e) F. Lancia, A. Ryabchun, N. Katsonis, *Nat. Rev. Chem.* **2019**, *3*, 536; f) D. Dattler, G. Fuks, J. Heiser, E. Moulin, A. Perrot, X. Yao, N. Giuseppone, *Chem. Rev.* **2020**, *120*, 310; g) M. Baroncini, S. Silvi, A. Credi, *Chem. Rev.* **2020**, *120*, 200; h) M. Jeong, J. Park, S. Kwon, *Eur. J. Org. Chem.* **2020**, *2020*, 7254; i) A. Perrot, E. Moulin, N. Giuseppone, *Trends Chem.* **2021**, *3*, 926; j) A. Mondal, R. Toyoda, R. Costil, B. L. Feringa, *Angew. Chem., Int. Ed.* **2022**, *61*, e202206631.
[4] a) V. Garcia-López, D. Liu, J. M. Tour, *Chem. Rev.* **2020**, *120*, 79; b) D. R. S. Pooler, A. S. Lubbe, S. Crespi, B. L. Feringa, *Chem. Sci.* **2021**, *12*, 14964.
[5] a) E. Moulin, L. Faour, C. C. Carmona-Vargas, N. Giuseppone, *Adv. Mater.* **2020**, *32*, 1906036; b) Q. Zhang, D.-H. Qu, H. Tian, B. L. Feringa, *Matter.* **2020**, *3*, 355; c) F. Xu, B. L. Feringa, *Adv. Mater.* **2023**, *35*, 2204413.
[6] a) A. Ryabchun, F. Lancia, J. Chen, D. Morozov, B. L. Feringa, N. Katsonis, *Adv. Mater.* **2020**, *32*, 2004420; b) J. Hou, A. Mondal, G. Long, L. de Haan, W. Zhao, G. Zhou, D. Liu, D. J. Broer, J. Chen, B. L. Feringa, *Angew. Chem., Int. Ed.* **2021**, *60*, 8251; c) J. Hou, G. Long, W. Zhao, G. Zhou, D. Liu, D. J. Broer, B. L. Feringa, J. Chen, *J. Am. Chem. Soc.* **2022**, *144*, 6851; d) A. Ryabchun, F. Lancia, J. Chen, R. Plamont, D. Morozov, B. L. Feringa, N. Katsonis, *Chem.* **2023**, *9*, 3544.
[7] a) D. J. van Dijken, J. Chen, M. C. Stuart, L. Hou, B. L. Feringa, *J. Am. Chem. Soc.* **2016**, *138*, 660; b) J. Chen, F. K. Leung, M. C. A. Stuart, T. Kajitani, T. Fukushima, E. van der Giessen, B. L. Feringa, *Nat. Chem.* **2018**, *10*, 132; c) D. Daou, Y. Zarate, M. Maaloum, D. Collin, G. Fleith, D. Constantin, E. Moulin, N. Giuseppone, *Adv. Mater.* **2024**, 2311293.
[8] a) Q. Li, G. Fuks, E. Moulin, M. Maaloum, M. Rawiso, I. Kulic, J. T. Foy, N. Giuseppone, *Nat. Nanotechnol.* **2015**, *10*, 161; b) J. T. Foy, Q. Li, A. Goujon, J. R. Colard-Itte, G. Fuks, E. Moulin, O. Schiffmann, D. Dattler, D. P. Funeriu, N. Giuseppone, *Nat. Nanotechnol.* **2017**, *12*, 540; c) J. R. Colard-Itte, Q. Li, D. Collin, G. Mariani, G. Fuks, E. Moulin, E. Buhler, N. Giuseppone, *Nanoscale.* **2019**, *11*, 5197; d) G. Mariani, J. R. Colard-Itte, E. Moulin, N. Giuseppone, E. Buhler, *Soft Matter.* **2020**, *16*, 4008; e) A. Perrot, W. Z. Wang, E. Buhler, E. Moulin, N. Giuseppone, *Angew. Chem., Int. Ed.* **2023**, *62*, e202300263.
[9] a) T. Sakai, T. Matsunaga, Y. Yamamoto, C. Ito, R. Yoshida, S. Suzuki, N. Sasaki, M. Shibayama, U.-i. Chung, *Macromolecules.* **2008**, *41*, 5379; b) M. Asai, T. Katashima, U.-i. Chung, T. Sakai, M. Shibayama, *Macromolecules.* **2013**, *46*, 9772; c) S. Nakagawa, N. Yoshie, *Polym. Chem.* **2022**, *13*, 2074; d) K. Nishi, H. Asai, K. Fujii, Y.-S. Han, T.-H. Kim, T. Sakai, M. Shibayama, *Macromolecules.* **2014**, *47*, 1801; e) M. Shibayama, X. Li, T. Sakai, *Colloid Polym. Sci.* **2019**, *297*, 1.
[10] a) B. M. Rosen, V. Percec, *Chem. Rev.* **2009**, *109*, 5069; b) S. R. Samanta, R. Cai, V. Percec, *J. Polym. Sci., Part A: Polym. Chem.* **2015**, *53*, 294; c) A. Anastasaki, V. Nikolaou, G. Nurumbetov, P. Wilson, K. Kempe, J. F. Quinn, T. P. Davis, M. R. Whittaker, D. M. Haddleton, *Chem. Rev.* **2016**, *116*, 835; d) A. Anastasaki, V. Nikolaou, D. M. Haddleton, *Polym. Chem.* **2016**, *7*, 1002; e) K. Matyjaszewski, *Adv. Mater.* **2018**, *30*, 1706441; f) G. R. Jones, A. Anastasaki, R. Whitfield, N. Engelis, E. Liarou, D. M. Haddleton, *Angew. Chem., Int. Ed.* **2018**, *57*, 10468; g) G. Creusen, A. Roshanasan, J. G. Lopez, K. Peneva, A. Walther, *Polym. Chem.* **2019**, *10*, 3740; h) K. Parkatzidis, H. S. Wang, N. P. Truong, A. Anastasaki, *Chem.* **2020**, *6*, 1575; i) F. Lorandi, M. Fantin, K. Matyjaszewski, *J. Am. Chem. Soc.* **2022**, *144*, 15413.
[11] N. Giuseppone, A. Walther, *Out-of-Equilibrium (Supra)molecular Systems and Materials*, Wiley-VCH, Weinheim **2021**.
[12] N. Koumura, E. M. Geertsema, M. B. van Gelder, A. Meetsma, B. L. Feringa, *J. Am. Chem. Soc.* **2002**, *124*, 5037.
[13] a) V. Percec, A. V. Popov, E. Ramirez-Castillo, M. Monteiro, B. Barboiu, O. Weichold, A. D. Asandei, C. M. Mitchell, *J. Am. Chem. Soc.* **2002**, *124*, 4940; b) V. Percec, T. Guliashvili, J. S. Ladislaw, A. Wistrand, A. Stjerndahl, M. J. Sienkowska, M. J. Monteiro, S. Sahoo, *J. Am. Chem. Soc.* **2006**, *128*, 14156; c) M. E. Levere, N. H. Nguyen, H.-J. Sun, V. Percec, *Polym. Chem.* **2013**, *4*, 686.
[14] A. Walther, A. S. Goldmann, R. S. Yelamanchili, M. Drechsler, H. Schmalz, A. Eisenberg, A. H. E. Müller, *Macromolecules.* **2008**, *41*, 3254.
[15] X. Huang, S. Nakagawa, X. Li, M. Shibayama, N. Yoshie, *Angew. Chem., Int. Ed.* **2020**, *59*, 9646.
[16] F. Kienberger, V. P. Pastushenko, G. Kada, H. J. Gruber, C. Riener, H. Schindler, P. Hinterdorfer, *Single Mol.* **2000**, *1*, 123.
[17] T. Li, H. Li, H. Wang, W. Lu, M. Osa, Y. Wang, J. Mays, K. Hong, *Polymer.* **2021**, *213*, 123207.

[18] S. K. Sukumaran, G. Beaucage, *EPL.* **2002**, *59*, 714.
[19] M. P. Allen, D. J. Tildesley, *Computer Simulation of Liquids*, Oxford University Press, Oxford **2017**.
[20] K. Kremer, G. S. Grest, *J. Chem. Phys.* **1990**, *92*, 5057.
[21] a) F. Weysser, O. Benzerara, A. Johner, I. M. Kulic, *Soft Matter.* **2015**, *11*, 732; b) J. D. Evans, S. Krause, B. L. Feringa, *Faraday Discuss.* **2021**, *225*, 286.
[22] J. H. Marden, L. R. Allen, *Proc. Natl. Acad. Sci. U. S. A.* **2002**, *99*, 4161.
[23] T. Hölzl, C. Mesner, M. Wittkop, S. Kreitmeier, S. Kain, D. Göritz, *Comput. Theor. Polym. Sci.* **1999**, *9*, 99.
[24] C. Gao, A. Vargas Jentzsch, E. Moulin, N. Giuseppone, *J. Am. Chem. Soc.* **2022**, *144*, 9845.
[25] M. Zhang, M. Fan, S. Peng, J. He, M. Deng, P. Gong, K. Wang, X. Zhang, *RSC Adv.* **2021**, *11*, 1605.